PH4100: Major Project
Equation of State:
For Hard & Soft Sphere Fluids

Name: Gregory Mikniche
Supervisor: Prof D Heyes

March, 2013

Abstract

We review equations of state that have been developed for the hard sphere, from the virial equation to the Carnahan-Starling approach. The latter using a closed form of the virial series, which approximates the higher order virial coefficients. Le Fevre suggested that for the hard sphere the virial equation should extrapolate to the random closed packing fraction. Using these idea we develop our own soft sphere equation of state, which has the ability to scale for the hard sphere case ($n \to \infty$) as well. We demonstrate that the equation is quite a good approximation in the hard sphere limit, and for $n = 32$ as it predicts random closed packing reasonably well.

Contents

1 Introduction

There are several equations of state (EOS) which describe many different types of matter very accurately. The hard sphere EOS is generally believed to be understood very well. Several EOS throughout the last century ventured to calculate successively higher terms of the virial series to increase the accuracy of the equation. Due to the nature of these virial EOS they become more accurate with each virial coefficient added, however, each virial coefficient (especially after the 5th or 6th) becomes increasingly more complicated to compute due to the increasing amount of cluster integrals. So naturally the search for a closed form EOS was important. The closed form equations devised came in many shapes and sizes, with even the simplest ones proving remarkably accurate.

1.1 Hard Sphere Equations of State

The hard sphere potential is defined by:

$$\Phi(r) = \begin{cases} \infty & r < \sigma \\ 0 & r \geq \sigma \end{cases} \tag{1}$$

Where Φ is the pair potential, and r the distance between two spheres, with diameter σ.

Some of the EOS's talked about below use the aforementioned virial series coefficients, which comes from the virial expansion EOS. It can be defined in the following way [6]:

$$Z = \frac{pV}{Nk_BT} = 1 + \sum_{m=2}^{\infty} B_m(T)\rho^{m-1} \tag{2}$$

Where Z is the compressibility factor, p pressure, V volume, N number of particles, k_B Boltzmann constant, T temperature, B_m mth virial coefficient and ρ number density[1]. The series can also be expressed as a function of the the packing fraction ζ, which is more useful for fluid states.

$$Z = 1 + \sum_{m=2}^{\infty} b_m\zeta^{m-1} \tag{3}$$

Where b_m are the 'reduced' virial coefficients. The first three terms of this infinite power series are given by:

$$Z = 1 + b_2\zeta + b_3\zeta^2 + ... \tag{4}$$

Where ζ is the packing fraction of the given hard sphere. We stopped at the third term here, however, with each higher order virial coefficient, B_m, calculated the equation becomes even more accurate. The virial coefficients themselves depend on particle interactions within a system. For example, the second coefficient, B_2, for the hard sphere indicates the breakdown from the ideal gas law[2], since it accounts for the pair interaction between particles.

$$B_2 = \frac{2\pi\sigma^3}{3} \tag{5}$$

The hard sphere virial coefficients are unique because they are temperature independent. Moreover, the second virial coefficient, B_2, for example, is dependant on only the hard core

[1] $\rho = \frac{N}{V}$
[2] $pV = Nk_BT$

diameter, σ. Clisby and McCoy[2] recently calculated up to the 10th virial coefficient. We can now look at the relative magnitude of the coefficients compared with B_2.

B_m/B_2	Relative virial coefficient
B_2/B_2	1
B_3/B_2^2	0.625
B_4/B_2^3	0.2869495
B_5/B_2^4	0.110252
B_6/B_2^5	0.03888198
B_7/B_2^6	0.01302354
B_8/B_2^7	0.0041832
B_9/B_2^8	0.0013094
B_{10}/B_2^9	0.0004035

Table 1: Tabulated data of the relative virial coefficients up to B_{10} as calculated by Clisby and McCoy. The coefficients have been divided by B_2^{n-1} in order to get a size, relative to B_2, of each coefficient for ease of comparison.

We can see the terms become significantly smaller as the virial series increases, so much that so that it is reasonable to look at approximated, closed and truncated forms of the virial EOS.

1.1.1 Carnahan-Starling

The Carnahan-Starling (CS) EOS for hard spheres[3] in their fluid phase is given by:

$$Z = \frac{pV}{Nk_BT} = \frac{1 + \zeta + \zeta^2 - \zeta^3}{(1-\zeta)^3}. \tag{6}$$

Where Z is the compressibility factor, p pressure, V volume, N number of particles, k_B Boltzmann constant, T temperature and ζ packing fraction of the given hard sphere. At the time or writing this (1969) only the first five virial coefficients were known to Carnahan and Starling: $B_2 = 4$, $B_3 = 10$, $B = 18$, $B_4 = 28$ and $B_5 = 40$. In this rounded form they were able to find a relation $n(n+3)$ that fit this data. Upon the assumption that this relation was also accurate for the higher virial coefficients, they formed a general expression of the virial coefficient:

$$B_n = \frac{(n-1)(n+2)}{4^{n-1}} b^{n-1} \tag{7}$$

We can compare the accuracy of this assumption with the data provided by Clisby and McCoy in.

B_m/B_2	Carnahan-Starling	Clisby and McCoy
B_2/B_2	1	1
B_3/B_2^2	0.625	0.625
B_4/B_2^3	0.2869495	0.28125
B_5/B_2^4	0.110252	0.109375
B_6/B_2^5	0.03888198	0.0390625
B_7/B_2^6	0.01302354	0.0131836
B_8/B_2^7	0.0041832	0.00427246
B_9/B_2^8	0.0013094	0.00134277
B_{10}/B_2^9	0.0004035	0.000411987

Table 2: Tabulated data of the relative virial coefficients up to B_{10} as calculated by CS, compared with data from Clisby and McCoy. The coefficients have been divided by B_2^{n-1} in order to get a size, relative to B_2, of each coefficient for ease of comparison.

The CS assumption seems quite justified as it is correct to two or more significant figures for $B_2 - B_7$ and B_9, and to one significant figure for B_8 and B_{10}. Therefore the CS EOS is a very good closed form of the virial EOS, especially as the coefficients that it does predict to poorer accuracy have less of an effect on the outcome of the equation, since the higher order terms are getting vastly smaller[3].

1.1.2 Le Fevre

Le Fevre [5] suggested that the virial series equation should extrapolate to the random closed packing fraction $\zeta^{RCP} = 0.64$ on a graph of inverse compressibility $1/Z$ as a function of the packing fraction ζ. The EOS he developed was as follows:

$$Z = \frac{1 + \alpha_3\zeta}{(1 + \alpha_1\zeta)(1 + \alpha_2\zeta)(1 + \beta_1\zeta + \gamma_1\zeta^2)(1 + \beta_2\zeta + \gamma_2\zeta^2)} \tag{8}$$

Where α_n, β_n and γ_n are constants and all other symbols have their usual definitions. The success of this EOS and its extrapolation of the random closed packing, led to a series of EOS's being proposed. However, it has been suggested that the virial series doesn't extrapolate to the hard sphere RCP fraction but instead to the fluid-crystal freezing transition [1] (i.e. the crystalline close packing density).

1.2 Soft Sphere Equations of State

The soft sphere potential is defined by:

$$\Phi(r) = \begin{cases} \epsilon\left(\frac{\sigma}{r}\right)^n & r \leq \sigma \\ 0 & r > \sigma \end{cases} \tag{9}$$

[3] As this is an infinite power series the first few, larger, virial coefficients dominate the expression to some degree.

Where ϵ is the interaction strength, n represents the stiffness of the potential (i.e. to what degree a sphere is hard or soft) and all other symbols have their usual definitions. This potential has worked well for a multitude of particles, including those in the hard sphere limit as $n \to \infty$ and $n = 36$, where the diameters of the spheres are close to that associated with the excluded volume of the particles. For small n, however, the particles become much softer and below $n \leq 3$, thermodynamically unstable.

For the soft sphere cases, it is important to look at the most accurate form of termination of the virial equation, since the softer particles are much more sensitive to the terms of the virial series. A few groups have used Padé approximates [7] in order to more accurately predict the convergence of the series, these produce much more complicated forms of the EOS, which have to be retuned for each soft sphere n.

$$Z[n=6] = \frac{1 + 7.432255\rho + 23.854807\rho^2 + 40.330195\rho^3 + 34.393896\rho^4 + 10.723480\rho^5}{1 + 3.720037\rho + 4.493218\rho^2 + 1.554135\rho^3} \tag{10}$$

$$Z[n=9] = \frac{1 + 3.098829\rho + 5.188915\rho^2 + 5.019851\rho^3 + 2.673385\rho^4 + 0.601529\rho^5}{1 + 0.262771\rho + 0.168052\rho^2 - 0.010554\rho^3} \tag{11}$$

These EOS's were developed by Tan et al. [7] and represent an accurate closed approximation of the EOS for $n = 6$ and $n = 9$ respectively. However, the goal of this project is to develop a so called 'simple' EOS, based on the ideas from Le Fevre. It should be simple in so far as the equation should be completely general over all n including the hard sphere limit ($n \to \infty$). It is the apparent simplicity associated with such equations of states as the CS that motivates us to develop it for the soft sphere.

2 Theory

Let us first look at the relationship between the compressibility factor Z and the the packing fraction ζ, this will give us some indication as to what the EOS should look like. The data sets used were all generously provided by direct correspondence with D. M. Heyes with the exception of the hard sphere data by Bannerman et al. [1], the raw form of these data sets can be made available upon request.

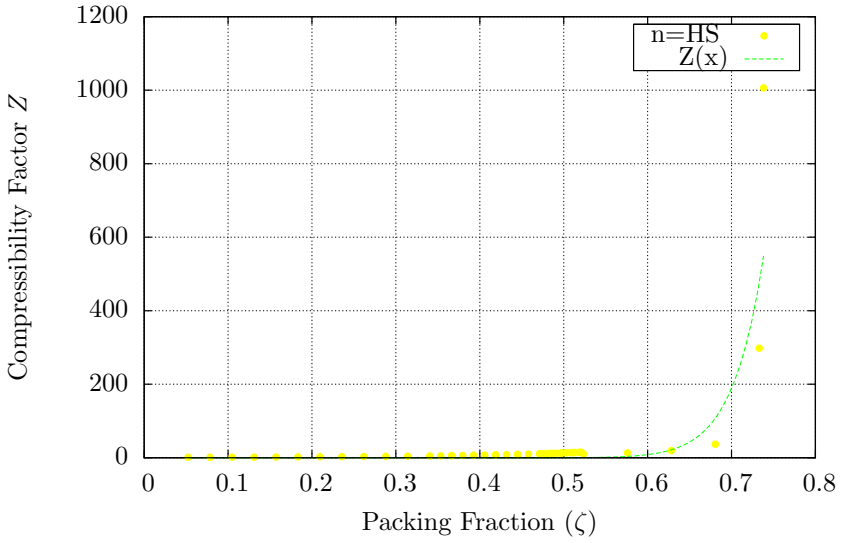

Figure 1: Compressibility Z as a function of the packing fraction ζ for the hard sphere potential.

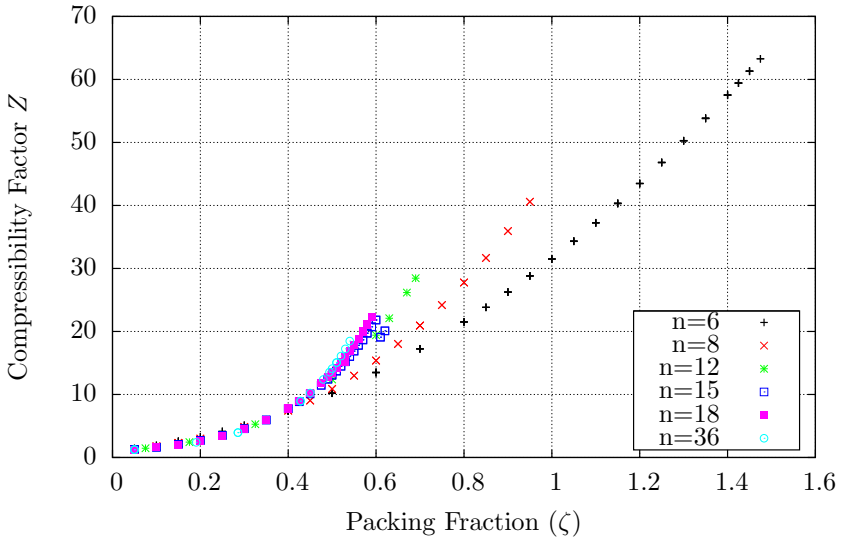

Figure 2: Compressibility Z as a function of the packing fraction ζ for softer potentials with $n = 6, 8, 12, 15, 18, 36$ as labelled in the key of the graph.

We can see that the function follows some sort of exponential, in the classical hard sphere case for instance this is clearly evident. The softer spheres were plotted separately from the hard sphere case, since, when they were plotted together, the hard sphere data dominated the graph region due to the much higher values of compressibility factor Z. The soft sphere graph shows similar relationships as in the hard sphere case, however as the potential becomes less stiff (i.e. particles become softer) the steepness of the curve eases. Furthermore, even plotted in this way, we can see each curve on the graph shares similar characteristics

and it is apparent that the stiffness n of each curve shares some obvious dependance on the steepness. Hence, if we can determine the dependance then we should be able to incorporate it into an equation of state.

2.1 Modifying the Equation of State

We used Le Fevre's ideas and his EOS (eq. (8)) as a starting point, as discussed earlier it's very good in the hard sphere limit, $n \to \infty$. We then modified it in an attempt to make it applicable to soft spheres too:

$$Z^c = \frac{A}{\zeta_i - \zeta} \tag{12}$$

The exponent term c represents a stiffness[4] scaling parameter, Z is the compressibility factor, A is a constant, ζ_i is a constant related to the packing fraction and ζ is simply the packing fraction. The importance of the power term is such that when $c = 1$, in the HS limit, we arrive back at a typical equation of state. Moreover, this approach allows us to extend the application of this equation to particles as soft as $n = 3$. Thus allowing us to apply potentials of both hard and soft spheres to a single EOS.

We understand that particles softer then $n = 3$ behave far too erratically then to be included in our model. In this region ($n \leq 3$) the potential gives rise to a non-diverging volume integral [4], such that the particles are no longer thermodynamically stable. It is for this reason why we will consider only particles whose potential satisfies $3 < n \leq \infty$, where the upper bound is, again, the hard sphere limit case.

The particular packing fraction ζ_i given in our EOS, would represent the random closed packing of hard spheres [8], $\zeta_{HS}^{RCP} = 0.6375$, in the hard sphere limit, $n \to \infty$. Furthermore, for softer particles, we can expect this ζ_i term to be equivalent to that of each particles own closed packing values. Thus, this makes a good reference for comparison with any previously calculated values. The packing fraction is given by, $\zeta = \pi\rho\frac{\sigma^3}{6}$, which represents the density of the particles, ρ.

Using the adapted equation of state (eq. (12)) we can now demonstrate the relationship between Z and ζ, in turn checking accuracy of the EOS. If we rearrange eq. (12), such that:

$$\zeta = \zeta_i - \frac{A}{Z^c} \tag{13}$$

We have the form of a straight line ($y = mx+c$), which allows us to plot the packing fraction ζ as a function of the inverse compressibility $1/Z^c$, giving us a y-intercept of the random closed packing fraction ζ_i and gradient of negative constant A. From this we will be able to check that the extrapolated values for the y-intercept ζ_i are consistent with other findings. Moreover, using Gnuplot's 'fit' command we will be able to extract the exponent c. This works by supplying the program with a given function, in this instance the straight line form of the EOS (eq. (13)), and a reasonable suggestion of the initial set of conditions for the constants of the function, for a set of data with stiffness n there are the corresponding constants ζ_i, A and exponent c. The program computes many iterations of the function

[4] How soft or hard a particular sphere is.

starting from these initial conditions until the best fit is found, leaving us with our values of the aforementioned constants. This can be repeated for each data set of varying stiffness n, in order to calculate each corresponding exponent c and extrapolated ζ_i. The graphs of which are viewable in the appendix.

It is promising to see a clear linear relationship between ζ and $1/Z^c$ in the graphs figs. 7 to 23 for each of the varying stiffnesses n. For the hard sphere case ($n \to \infty$) fig. 7 shows almost a completely linear relation with the exception of six points above $\zeta = 0.52$. These points represent the solid phase of the system and they follow a face centred cubic (FCC) path. Therefore, we can exclude these results from the fitting function and re-plot the graph, see fig. 8. This gives a straight line that fits the allowed data very well.

For the $n = 36$ case in fig. 9 there is a very a good straight line through all the points that extrapolates well onto the y-axis.

For the $n = 18$ case in fig. 10 it is hard to tell if the points fit the straight line at this resolution, but the y-intercept still extrapolates well. Focusing onto the region of interest in fig. 11 we observe the straight line is a very good fit through the vast majority of points.

For the $n = 15$ case in fig. 12 it is hard to tell how the points fit the straight at this resolution, but the y-intercept still extrapolates well. Focusing onto the region of interest in fig. 13 it shows that the straight line is a very good fit through the vast majority of points, with the exception of two points above $\zeta = 0.6$. This is due to the nucleation[5] of particles in the system, since if they are able to transition very quickly the system can move into a supercritical region. Therefore, we can exclude these results from the fitting function and re-plot the graph, see fig. 14. This produces a very good line of best that passes through the majority of the allowed data points.

For the $n = 12$ case in fig. 15 it is hard to tell how the points fit the straight at this resolution, but the y-intercept still extrapolates well. Focusing onto the region of interest in fig. 16 it shows that the straight line is a reasonable fit through the majority of points. However, four points lying above $\zeta = 0.6$ can be excluded due to nucleation, see fig. 17. This produces a very good line of best that passes through the majority of the allowed data points.

For the $n = 8$ case in fig. 18 it is hard to tell how the points fit the straight at this resolution, but the y-intercept still extrapolates well. Focusing onto the region of interest in fig. 19 it shows that the straight line is a poor fit for this data set. However, the best fit will present itself if we ignore the points below $\zeta = 0.3$ due to the particles being thermodynamically unstable, see fig. 20. This produces a very good line of best that passes through the majority of the allowed data points.

For the $n = 6$ case in fig. 21 it is hard to tell how the points fit the straight at this resolution, but the y-intercept still extrapolates well. Focusing onto the region of interest in fig. 22 it shows that the straight line is a poor fit for this data set. However, the best fit will present itself if we ignore the points below $\zeta = 0.6$ due to the particles being thermodynamically unstable, see fig. 23. This produces a very good line of best that passes through

[5]Formation of a nucleus.

the majority of the allowed data points.

A summary of the graphs can be seen in figs. 24 and 25, where we superimposed the different graphs over each other. Figure 24 contains the data without any of the points excluded and fig. 25 uses the excluded range data sets where possible. Although we are not able to see the individual points at this resolution, we can compare the extrapolated ζ_i values. For both sets of data we see ζ_i rising as n decreases (spheres becoming softer), with the exception of $n = 8$ which appears to extrapolate to a much lower value then predicted, i.e. between the y-intercepts of $n = 6, 12$. A key difference between the graphs, is that in the excluded data series set the ζ_i are much lower across the board, with the exception of the hard sphere case. This is due to limiting the range that ζ values can take when fitting the function, which was done to improve the accuracy of the fitting function[6] to each data set where necessary.

To better identify the points along the line we shall group a few of the stiffnesses, n, together, in turn increasing the resolution of the graphs around these points, see Figures 26 to 31. For the hardest spheres in our sample, $n = 18, 36$ and the hard sphere $n \to \infty$, we can see more clearly that the ζ_i values increase directly as the stiffness of the potential decreases. Furthermore, with comparison to fig. 27, which has the excluded values from the hard sphere data, we observe an increase in the random closed packing fraction for the hard sphere whilst the other fits remain the unperturbed. The ζ_i values for the hard sphere case ($\zeta_i^{HS} = 0.85266 \pm 0.03161$ and $\zeta_i^{HS_{ex}} = 1.26712 \pm 0.007457$) and to some extent the $n = 32$ case (1.46063 ± 0.004329) should match quite closely to the random closed packing fraction $\zeta^{RCP} = 0.64$. However, neither of these packing fractions are in concordance with the random closed packing value, although the hard sphere case is closest being only 33% away.

For the middle of the road spheres from our sample, $n = 12, 15, 18$, we observe that their ζ_i values are much higher then then in the hard sphere category above. Upon comparing the excluded values graph fit in fig. 29 with the fit from the unperturbed graph fig. 28, we notice that the fit is better in the $n = 12$ cases (i.e. line passes through more points) and yields a lower ζ_i value. Similar to the case of the hard sphere, for $n = 15$ the ζ_i value increases.

For the softest spheres from our sample, $n = 6, 8, 12$, we observe that their ζ_i values are higher still then then in the hard sphere and medium sphere categories above. It is apparent that $n = 8$ is an anomalous case again, being out of place in these graphs figs. 30 and 31 as it was in the superimposed plots (figs. 24 and 25), since its extrapolated fit line is predicted to rest between the two lines from $n = 6, 12$. Upon comparing the excluded values graph fit fig. 31 with the fit from the unperturbed graph fig. 30, we notice that the fits are better in all cases (i.e. pass through more points) and yield lower ζ_i values. Although it may appear as though the y-intercept for the $n = 12$ fit is larger then $n = 6$ in the excluded range plot, this is not the case, since the gradient is lower than the extrapolated line corresponding to $n = 6$ so its intercept will also be lower.

[6] Which relates to a better fitting line of best fit.

3 Dependance of n

It will be useful to tabulate the data discussed in the above section for ease of reference and discussion.

n	Intercept, ζ_i	Exponent, c	Intercept (excluded), ζ_i^{ex}	Exponent (excluded), c^{ex}
∞	0.85266	0.364485	1.26712	0.195709
32	1.46063	0.158	n/a	n/a
18	3.97214	0.0512813	n/a	n/a
15	9.86323	0.0204839	24.966	0.00779862
12	44.629	0.00463556	31.3361	0.00643993
8	22.8332	0.0113661	16.5088	0.0193647
6	64.0236	0.00615825	37.3109	0.0157428

Table 3: Tabulated data from the graphs discussed above (figs. 24 and 25 in the appendix). The excluded title corresponds to those data sets that had data ζ values cut-off in order to improve the fitting function.

We now seek to determine the dependance of n with the exponent and intercept of these graphs. This will allow us to rewrite these terms as a function of n, which can then be substituted into our final form of the EOS for hard and soft spheres.

3.1 On the Intercept ζ_i

It's clear that the y-intercept, ζ_i has a relationship with the inverse of stiffness, $1/n$, for a given potential. We chose to take the following equation as the form of this function, and used it as the 'fitting' function within Gnuplot similar to the previous instance.

$$\frac{1}{\zeta_i} = a + bx^{\beta} \tag{14}$$

With ζ_i as the y-intercept from before, x^{β} as a function of n with exponent β (different from exponent c) and a, b constants. As previously discussed particles are thermodynamically unstable in the $n \leq 3$ region, therefore x can be set as, $x(n) = \frac{1}{n} \Rightarrow \frac{1}{3} - \frac{1}{n}$, such that the function terminates in the unstable region[7]:

$$\frac{1}{\zeta_i} = a + b\left(\frac{1}{3} - \frac{1}{n}\right)^{\beta} \tag{15}$$

Which takes the form of a straight line, plotting $\frac{1}{\zeta_i}$ as a function of $\left(\frac{1}{3} - \frac{1}{n}\right)^{\beta}$.

[7] e.g. $n = 3 \rightarrow x = 1/3 - 1/3 = 0$

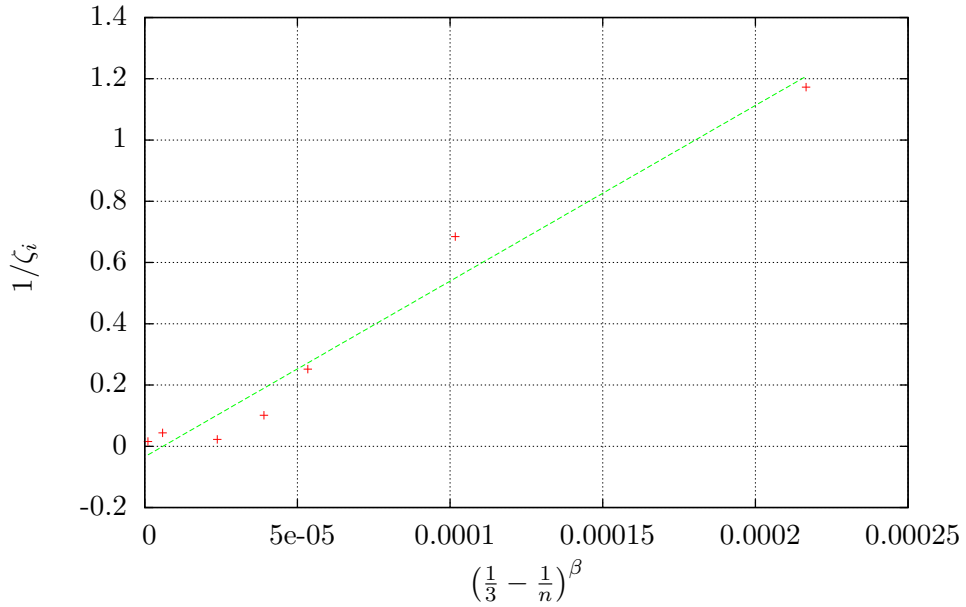

Figure 3: Graph of the inverse y-intercept, ζ_i from the previous graphs (see appendix) as a function of the inverse stiffness, n, corrected for thermodynamic stability.

This supports our proposed linear relationship in eq. (15) and shows it to be quite a good match. The y-intercept of the graph, $1/\zeta_i = -0.0342224 \pm 0.07712$, since that within error it passes through the origin comfortably it supports our exclusion of the thermodynamically unstable particles, $n \leq 3$. The exponent is given by, $\beta = 7.68006 \pm 1.663$.

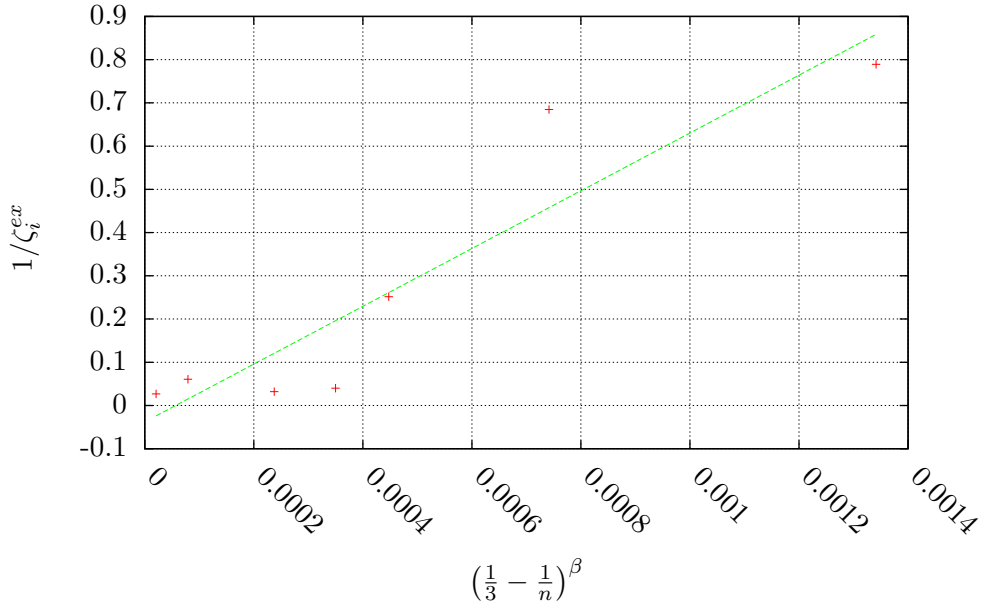

Figure 4: Same graph as fig. 3 using the excluded data for the y-intercept ζ_i.

This graph contains the excluded data where possible, for n where no cut-off was applied the unperturbed data was used instead (for $n = 18, 32$). The y-intercept of this graph, given the same fitting function, is $1/\zeta_i = -0.0379691 \pm 0.1439$, which like the unperturbed data also passes through the origin. However, the fitting function does not get as close to all points as in fig. 3, which shows that the cut-off point may be having a negative impact on the accuracy. The exponent is given by, $\beta = 6.02041 \pm 2.944$.

We observe that both exponents are equivalent, within the calculated error. This shows that the cut-off data, which was used in an attempt to improve the resulting functional fit, has a limited and perhaps hampering effect (not least because it reduces the accuracy of the extrapolation). Considering that fig. 4 is a poorer fit of the cut-off data, then it is in fig. 3 with the unperturbed data, we may conclude a few things. The cut-off data ranges chosen may not have been appropriate, either the cut-off range was not significant enough to warrant any distinct improvements over the unperturbed data, or was overly aggressive in eliminating data and so produced a poorer, less accurate fit. This withstanding, perhaps the cut-off approach was a poor method for improving the fitting functional in the first place, and more data could have been used instead to improve the accuracy of the extrapolation results. The long range associated with the extrapolated value for the y-intercept, ζ_i, brings about an inherent high degree of uncertainty with it. Therefore, the more points cut-off from the data set would only lead to an increase in this uncertainty, hence, a strong argument can be made for more data included in the plots.

3.2 On the Exponent c

It's clear that the exponent, c has a relationship with the inverse of stiffness, $1/n$, for a given particle. We chose to take the following equation as the form of this function, and used it as the 'fitting' function within Gnuplot similar to the previous instance.

$$c = a + bx^{\beta} \tag{16}$$

With c as the exponent from before, $x^{\beta} = \frac{1}{3} - \frac{1}{n}$ as a function of n with exponent γ (different from exponent c) and a, b constants. As previously discussed particles are thermodynamically unstable in the $n \leq 3$ region, therefore we set $x(n) = \frac{1}{3} - \frac{1}{n}$.

$$c = a + b\left(\frac{1}{3} - \frac{1}{n}\right)^{\gamma} \tag{17}$$

Which takes the form of a straight line, plotting c as a function of $\left(\frac{1}{3} - \frac{1}{n}\right)^{\gamma}$.

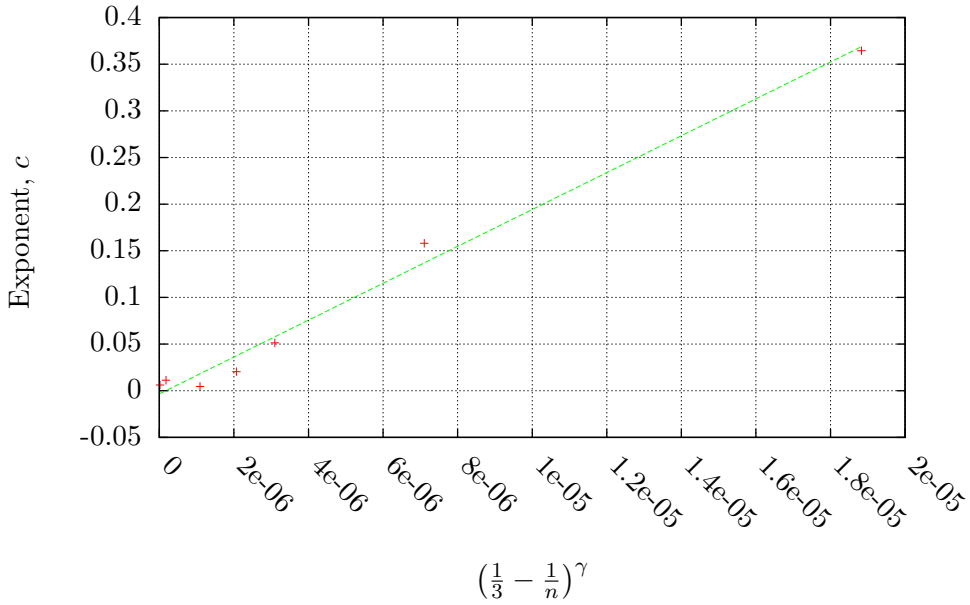

Figure 5: Graph of the exponent, c from the previous graphs (see appendix) as a function of the inverse stiffness, n, corrected for thermodynamic stability.

This supports our proposed linear relationship in eq. (17) and shows it to be an almost identical looking graph to that in fig. 3. The only difference between the two graphs appears to be one of scale, with this one having an x-range approximately an order of 10 smaller and y-range about 1/3 as much. The y-intercept of the graph, $1/\zeta_i = -0.0033799 \pm 0.01176$, since that within error it passes through the origin comfortably it supports the exclusion of the thermodynamically unstable particles ($n \leq 3$). The exponent is given by, $\gamma = 9.90339 \pm 1.296$.

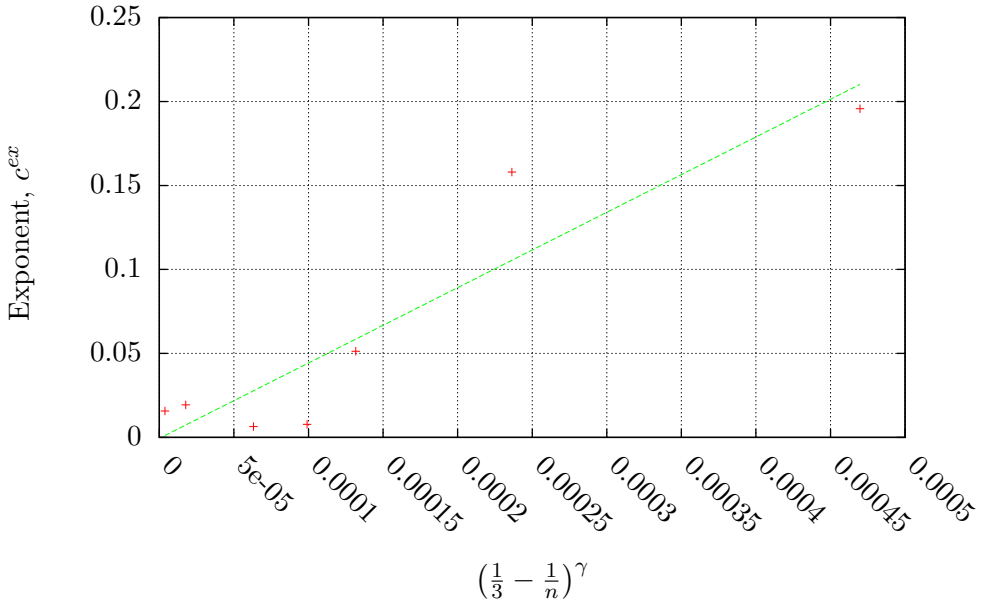

Figure 6: Same graph as fig. 3 using the excluded data for the exponent c.

This graph contains the excluded data where possible, for n where no cut-off was applied the unperturbed data was used instead (for $n = 18, 32$). The y-intercept of this graph, given the same fitting function, is $1/\zeta_i = -0.000567819 \pm 0.03019$, which like the unperturbed data also passes through the origin. However, the fitting function does not get as close to all points as in fig. 5, which shows that the cut-off point may be having a negative impact on the relationship. Similarly to the graph (using unperturbed data) above, this graph is practically identical to fig. 4, since the only difference lies in the axis scale; This graphs x-axis is roughly 3.5 times larger and y-axis about a third of its counterparts size. The exponent is given by, $\beta = 6.97543 \pm 3.295$.

4 Analysis

Taking a look at both relationships shown in figs. 3 to 6, it is clear that the exponents of these two graphs lie within the uncertainty of each other and thus we can take them as equivalent. As the graphs looking at the y-intercept relationship in figs. 3 and 4 are nearly identical to the graphs of exponent relationship in figs. 5 and 6, it follows that the we can make some of the same conclusions here as we did there. Predominantly, the discussion about the accuracy and usefulness of the cut-off data ranges also applies here. We think it is fair to say that the exponent terms β and γ for the two cases are within the uncertainty of each other, thus:

$$\kappa = \quad \beta \quad \equiv \quad \gamma \quad \approx 9$$

Such that our relations becomes:

$$\frac{1}{\zeta_i} = a + b\left(\frac{1}{3} - \frac{1}{n}\right)^{\kappa} \qquad (18) \qquad\qquad c = a + b\left(\frac{1}{3} - \frac{1}{n}\right)^{\kappa} \qquad (19)$$

We have shown graphically that these functions are equivalent, therefore:

$$c \propto \frac{1}{\zeta_i} \tag{20}$$

Which allows us to rewrite our EOS (eq. (13)) as:

$$\zeta = \zeta_i - \frac{A}{Z^c} = \zeta_i - \frac{A}{Z^{\frac{B}{\zeta_i}}} \tag{21}$$

Finally, rearranging to the same form as (eq. (12)):

$$Z^{\frac{B}{\zeta_i}} = \frac{A}{\zeta_i - \zeta} \tag{22}$$

$$Z = \left[\frac{A}{\zeta_i - \zeta}\right]^{\frac{\zeta_i}{B}} \tag{23}$$

Where B is the constant of proportionality from eq. (20).

5 Conclusion

In conclusion we have discussed the use of several hard sphere equations of state. With the root of them drawing from the virial expansion, where the virial coefficients are increasingly complex and non-trivial due to the number of cluster integrals involved in the higher order terms. The natural progression from here was to develop a closed form of the virial series, which makes an estimate of the higher order terms in the expansion. CS developed a widely accepted, and very successful, EOS based upon a pattern observed in a handful of the first virial coefficients B_n. Using this assumed expression of the virial coefficients we were able to compute the first ten and compare them to those produced recently by Clisby and McCoy. It showed us that this simple CS EOS is, to a large extent, remarkably over this region. Furthermore, we notice that the size of the virial coefficients is falling off rapidly after the first few terms, and so the approximations made about the higher coefficients are more justified.

From plotting the data of compressibility factor as a function of packing fraction, we were able to develop our on EOS based upon the ideas proposed by Le Fevre about the random closed packing extrapolation in the hard sphere limit. Our equation was modified by adding an exponent term c to the compressibility factor, in the hope that we can get this term to scale the equation depending on the sphere potential applied, wether it be soft or hard. The plots in the appendix demonstrate that the extrapolation works reasonably well for the hardest spheres, $n \to \infty$ and $n = 32$, as their ζ_i values are close to random closed packing $\zeta^{RCP} = 0.64$. It was clear on grouped plots **??** that their is an anomaly for the $n = 8$ case that is not well understood. Perhaps it was due to some error within the the plotting command, or maybe it shows that for soft spheres, which as discussed become thermodynamically unstable below $n = 3$, it is particular hard to develop a general equation of state to work well in this region. We implemented a cut-off on some of the data sets, in order to get a better fitting function, implying better exponents and extrapolated ζ_i values. However, this came at a cost of increasing the uncertainty in the extrapolated values, since the fit command has less points to work with, it is more sensitive to them.

Finally, we discussed the n dependance on both the exponent and the y-intercept. We found that they formed to two similar relationships, which was obvious from the graphs produced of this. They were nearly identical, with the exception on the scale of the x and y axis. The exponent used in each case was measured to be approximately $\kappa \approx 9$ for both functional forms. Although, not completed to its fullest, we have started to incorporate this finding into our equation of state eq. (23). But further work needs to be done in order to find the form of the exponent c.

6 References

[1] Marcus N Bannerman, Leo Lue, and Leslie V Woodcock. Thermodynamic pressures for hard spheres and closed-virial equation-of-state. *The Journal of Chemical Physics*, 132(8):084507, 2010.

[2] N Clisby and B M McCoy. Ninth and Tenth Order Virial Coefficients for Hard Spheres in D Dimensions. *Journal of Statistical Physics*, 122:15–57, 2006.

[3] Hendrik Hansen-Goos and Roland Roth. A new generalization of the Carnahan-Starling equation of state to additive mixtures of hard spheres. *The Journal of Chemical Physics*, 124(15):154506, 2006.

[4] D M Heyes, S M Clarke, and A C Branka. Soft-sphere soft glasses. *The Journal of Chemical Physics*, 131(20):204506, 2009.

[5] E J Le Fevre. Equation of State for Hard-sphere Fluid. *Nature Physical Science*, 235:20, 1972.

[6] Miguel Angel G Maestre, Andres Santos, Miguel Robles, and Mariano Lopez de Haro. On the relation between virial coefficients and the close-packing of hard disks and hard spheres. *The Journal of Chemical Physics*, 134(8):084502, 2011.

[7] Tai Boon Tan, Andrew J Schultz, and David A Kofke. Virial coefficients, equation of state, and solid–fluid coexistence for the soft sphere model. *Molecular Physics*, 109(1):123–132, 2011.

[8] Leslie V Woodcock. Thermodynamic description of liquid-state limits. *The journal of physical chemistry. B*, 116(12):3735–3744, March 2012.

Appendices

A Packing Fraction, ζ, vs $1/Z^c$

The following graphs are plots of packing fraction, ζ, as a function of the inverse compressibility raised to the stiffness scaling parameter exponent, Z^c, for different sphere stiffness, n.

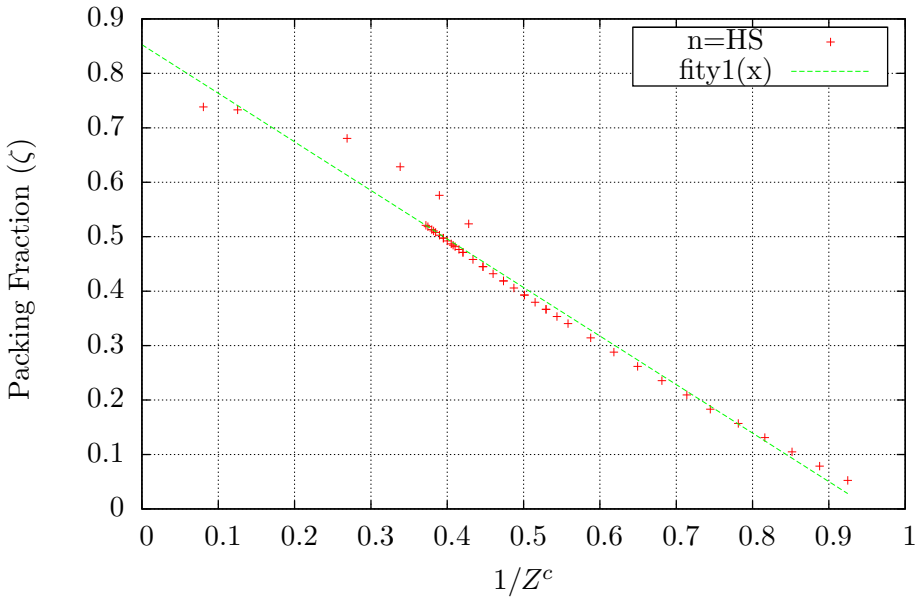

Figure 7: Graph of the hard sphere, $n \to \infty$

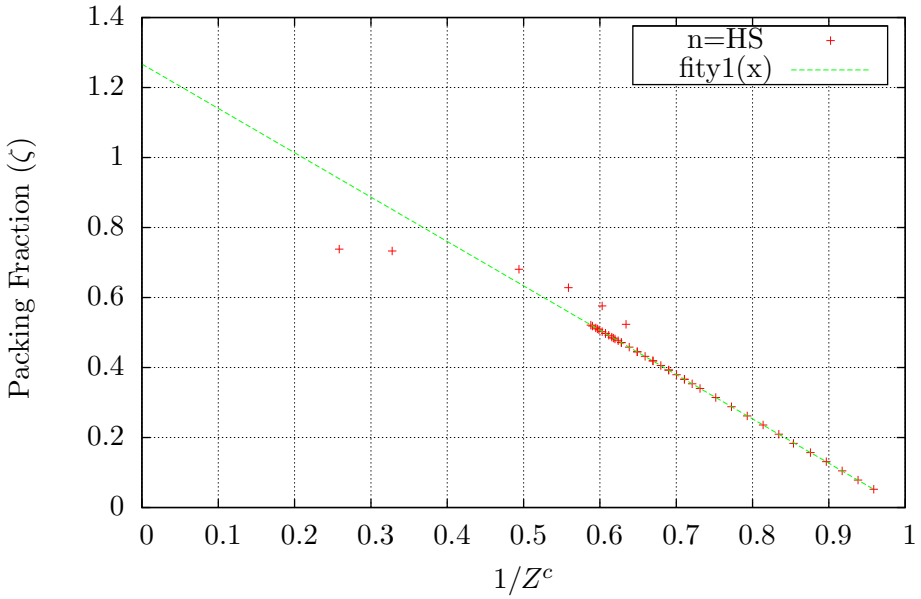

Figure 8: Same graph as fig. 7 with the nucleated points above $\zeta = 0.52$ excluded from the fitting range.

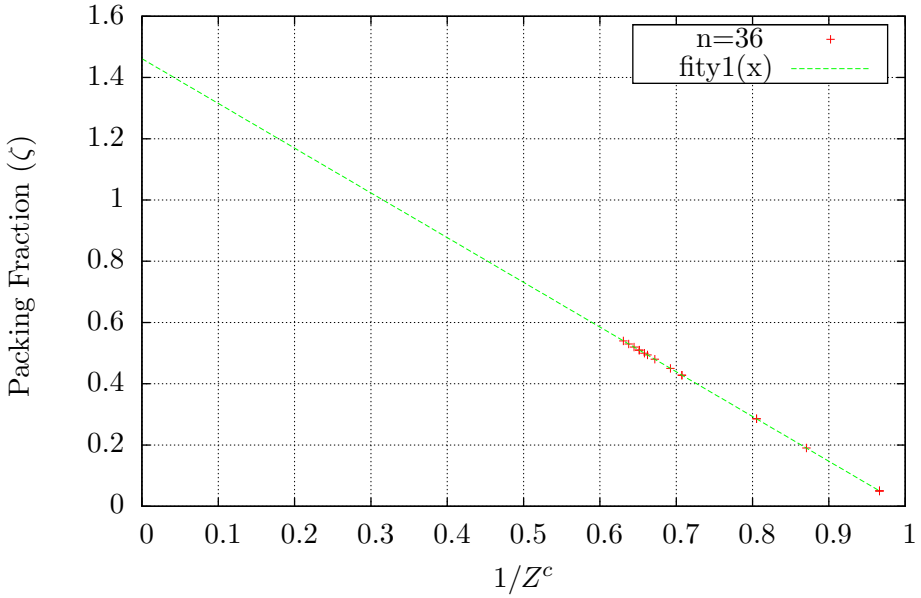

Figure 9: Graph of the soft sphere potential with stiffness $n = 36$

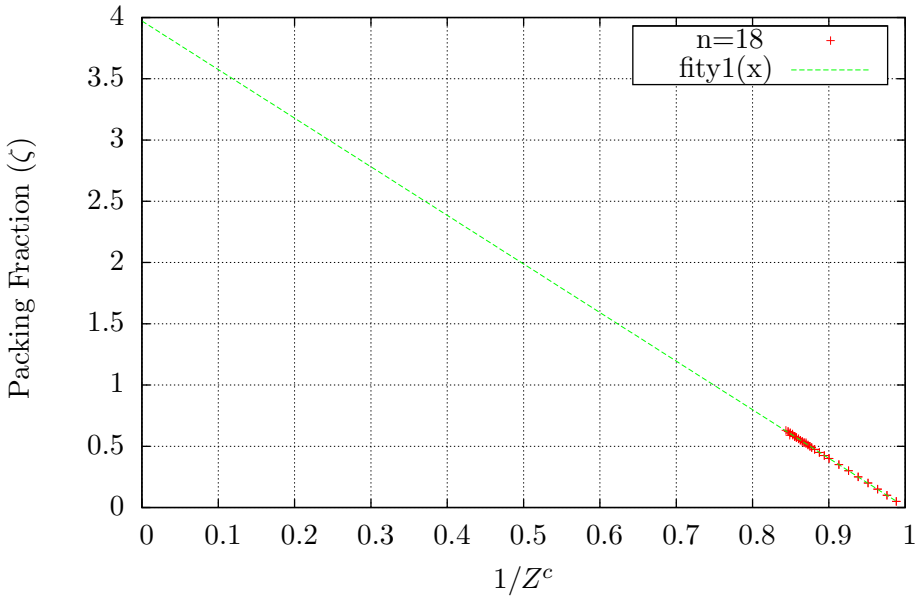

Figure 10: Graph of the soft sphere potential with stiffness $n = 18$

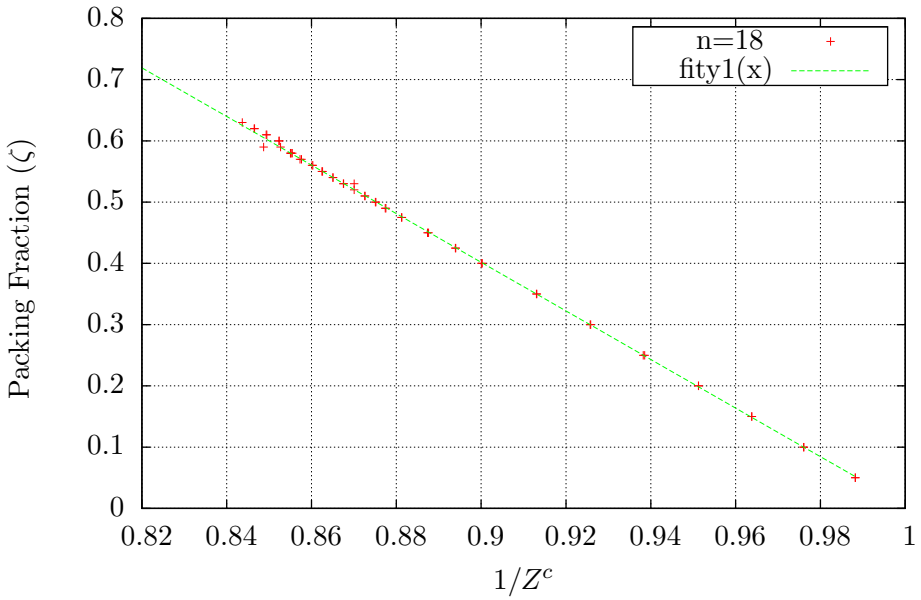

Figure 11: Same graph as fig. 10 with a zoomed view of the points of interest.

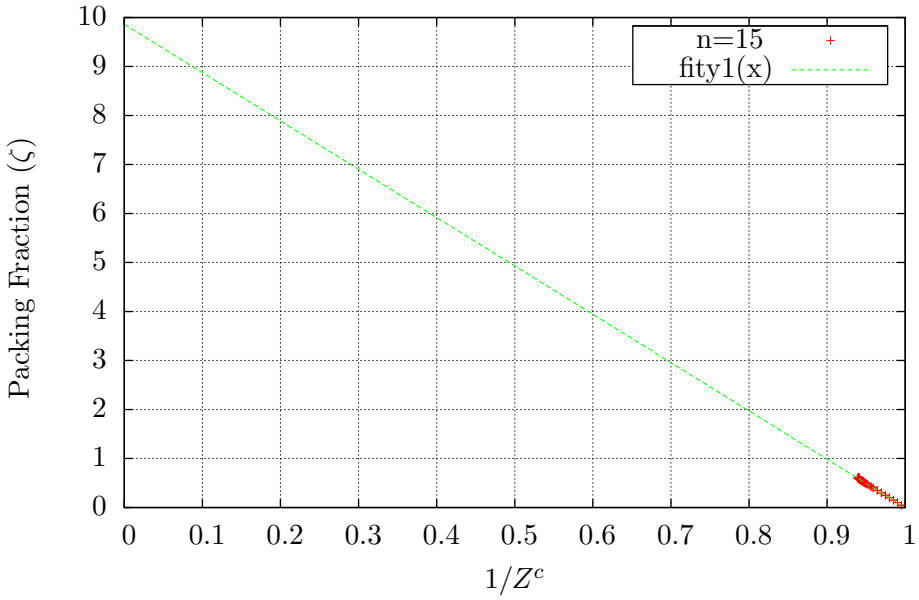

Figure 12: Graph of the soft sphere potential with stiffness $n = 15$

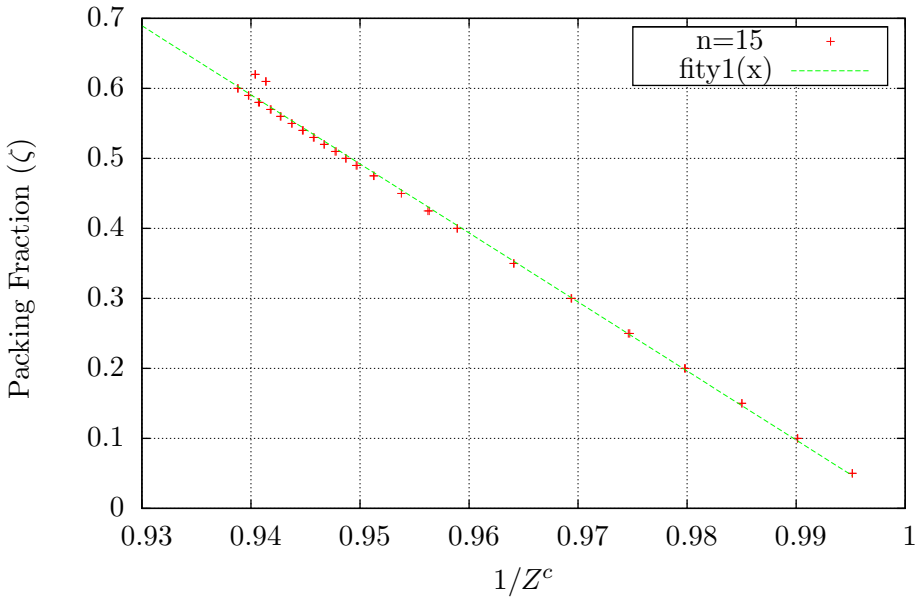

Figure 13: Same graph as fig. 12 with a zoomed view of the points of interest.

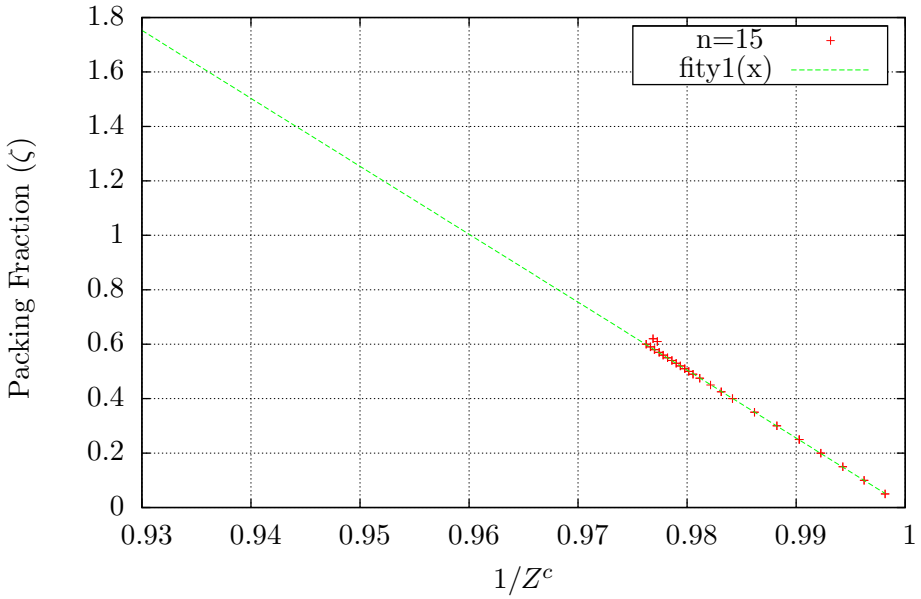

Figure 14: Same graph as fig. 13 with the nucleated points above $\zeta = 0.6$ excluded from the fitting range.

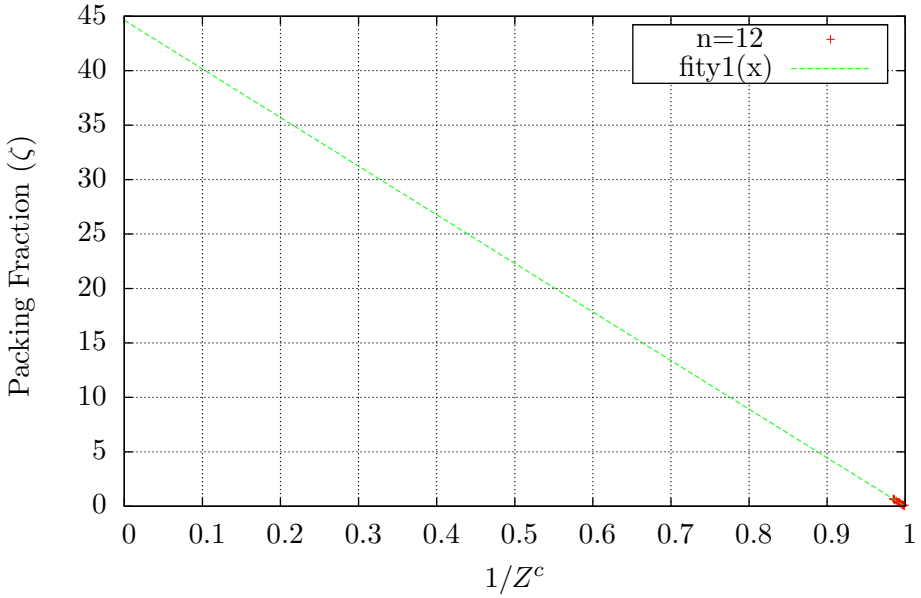

Figure 15: Graph of the soft sphere potential with stiffness $n = 12$

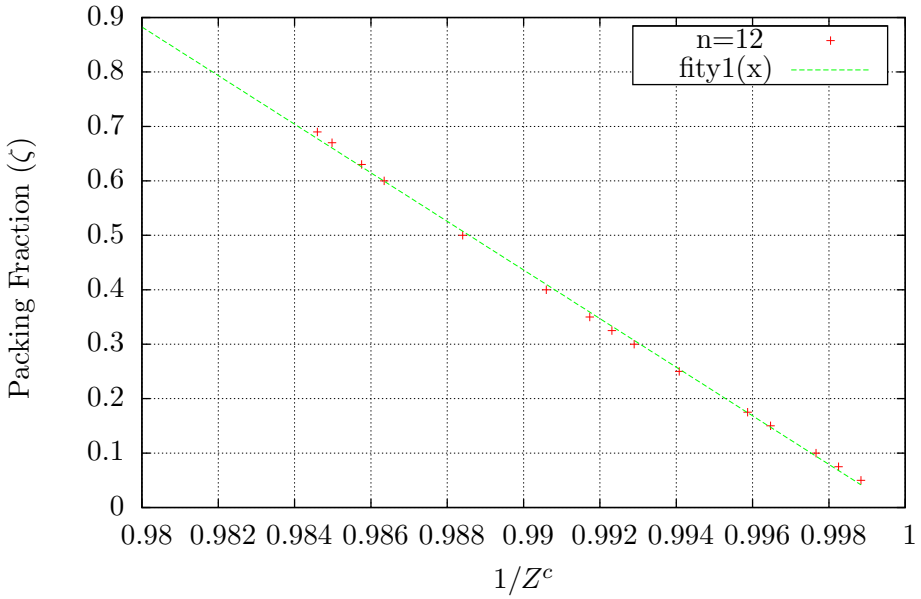

Figure 16: Same graph as fig. 15 with a zoomed view of the points of interest.

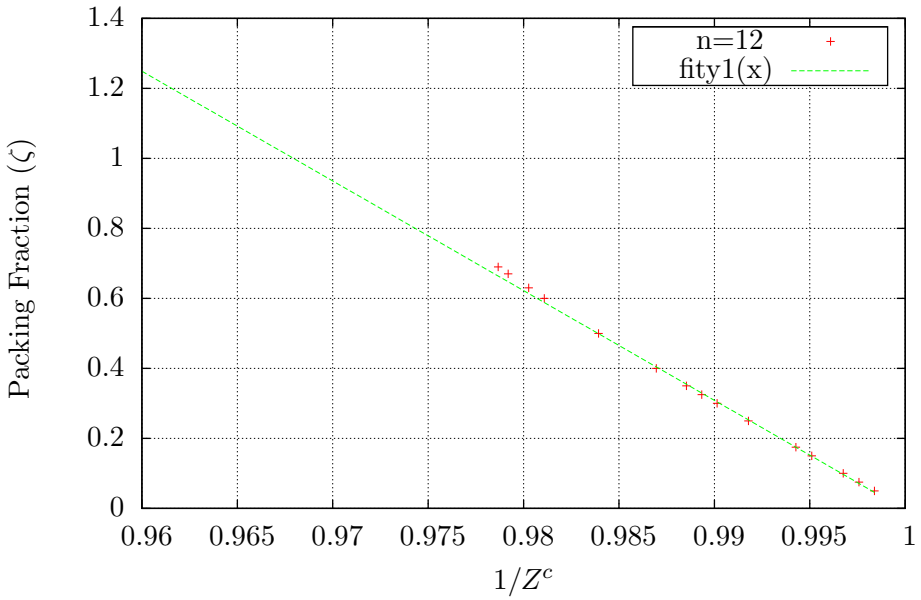

Figure 17: Same graph as fig. 16 with the nucleated points above $\zeta = 0.6$ excluded from the fitting range.

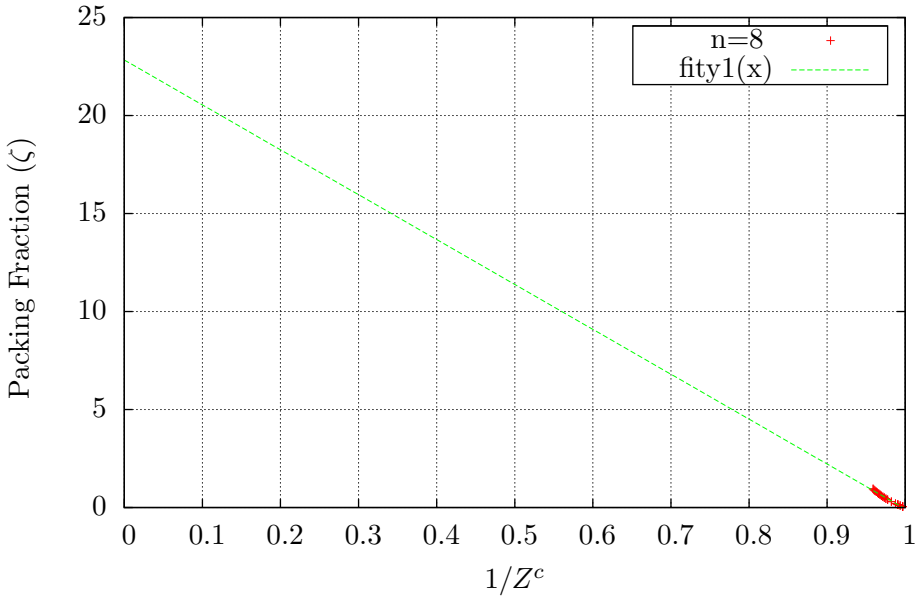

Figure 18: Graph of the soft sphere potential with stiffness $n = 8$

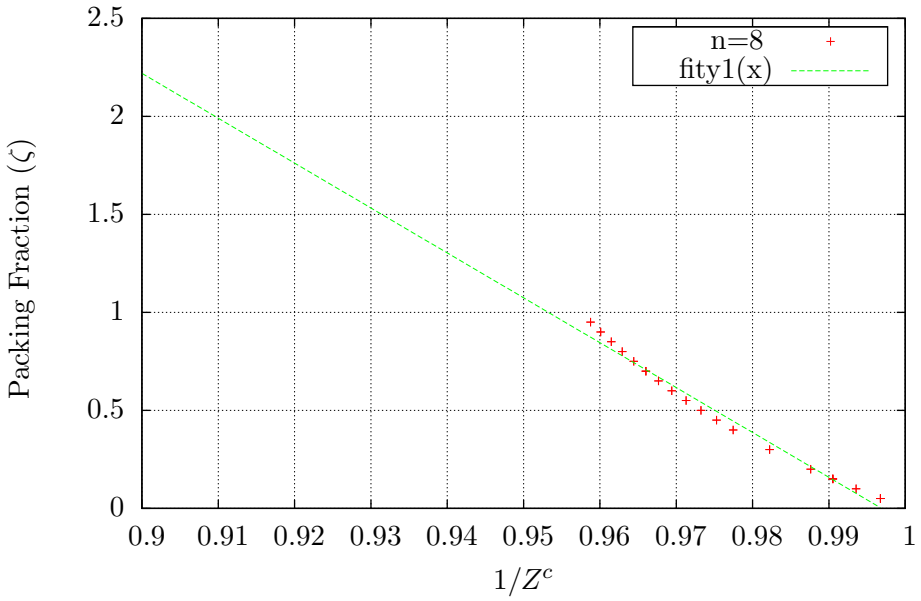

Figure 19: Same graph as fig. 18 with a zoomed view of the points of interest.

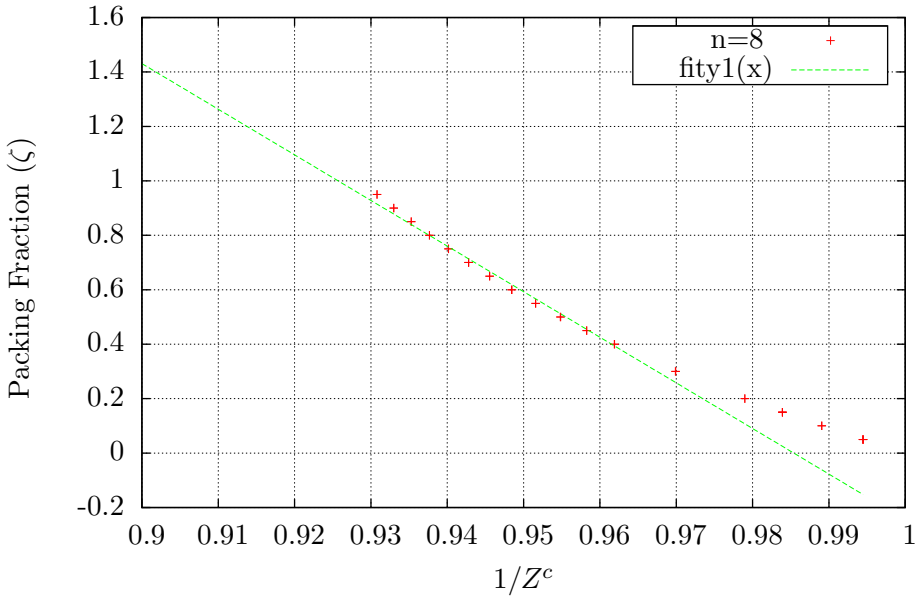

Figure 20: Same graph as fig. 19 with the points below $\zeta = 0.3$ excluded from the fitting range.

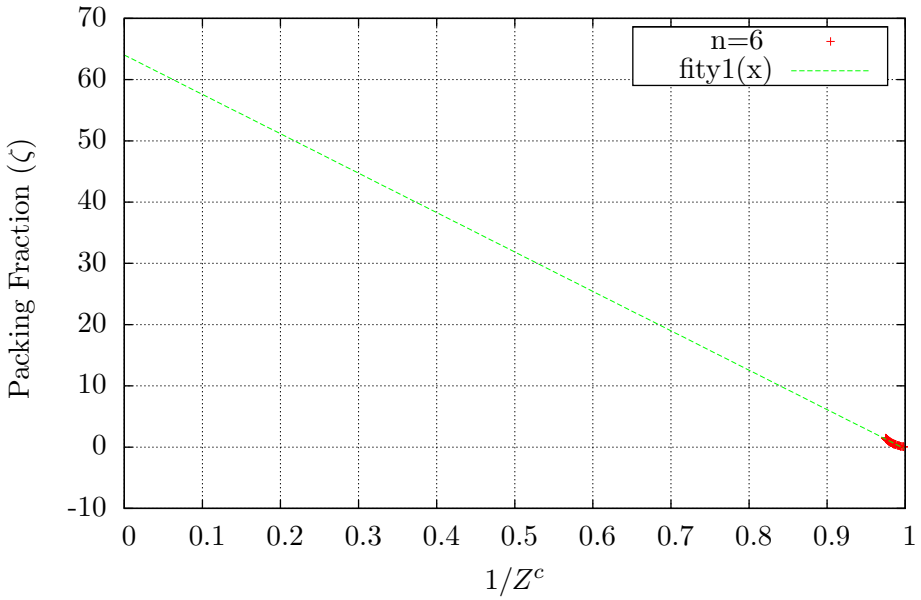

Figure 21: Graph of the soft sphere potential with stiffness $n = 6$

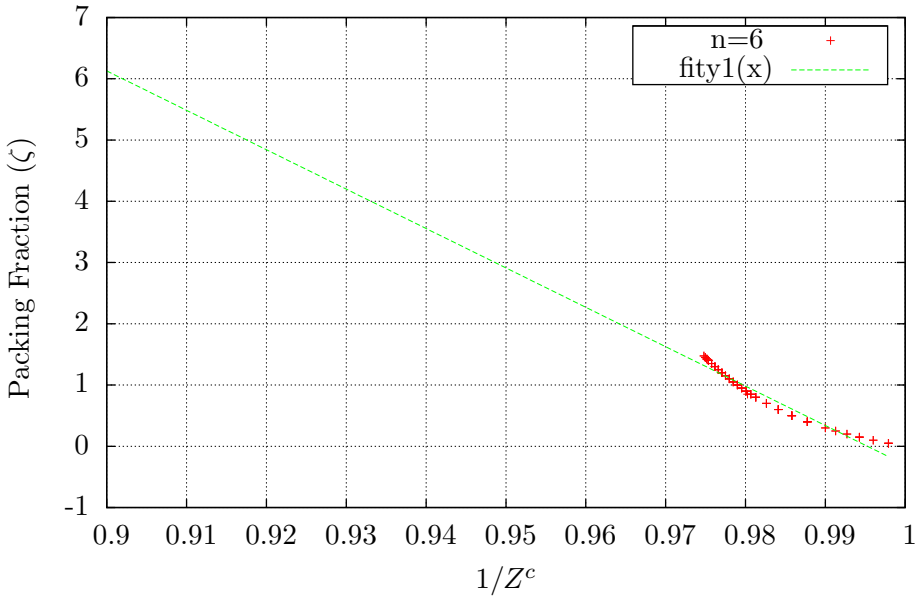

Figure 22: Same graph as fig. 21 with a zoomed view of the points of interest.

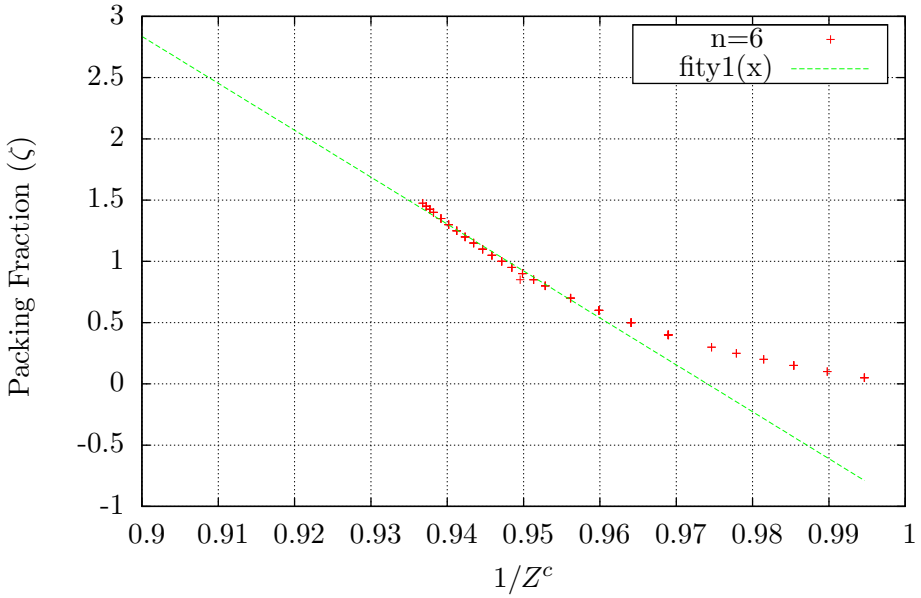

Figure 23: Same graph as fig. 22 with the points below $\zeta = 0.6$ excluded from the fitting range.

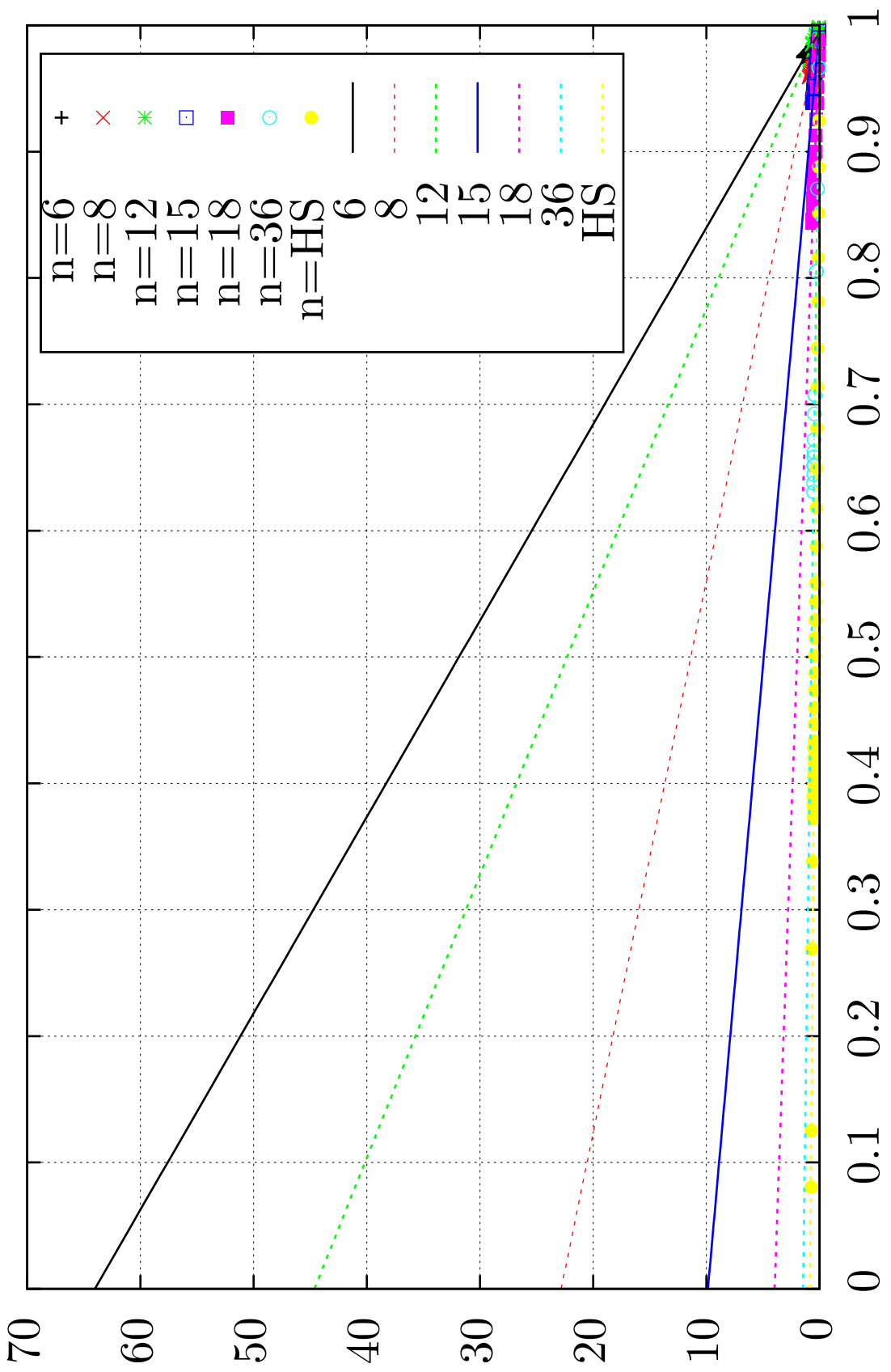

Figure 24: Superimposed graph of figs. 7, 9, 10, 12, 15, 18 and 21 over the complete data range.

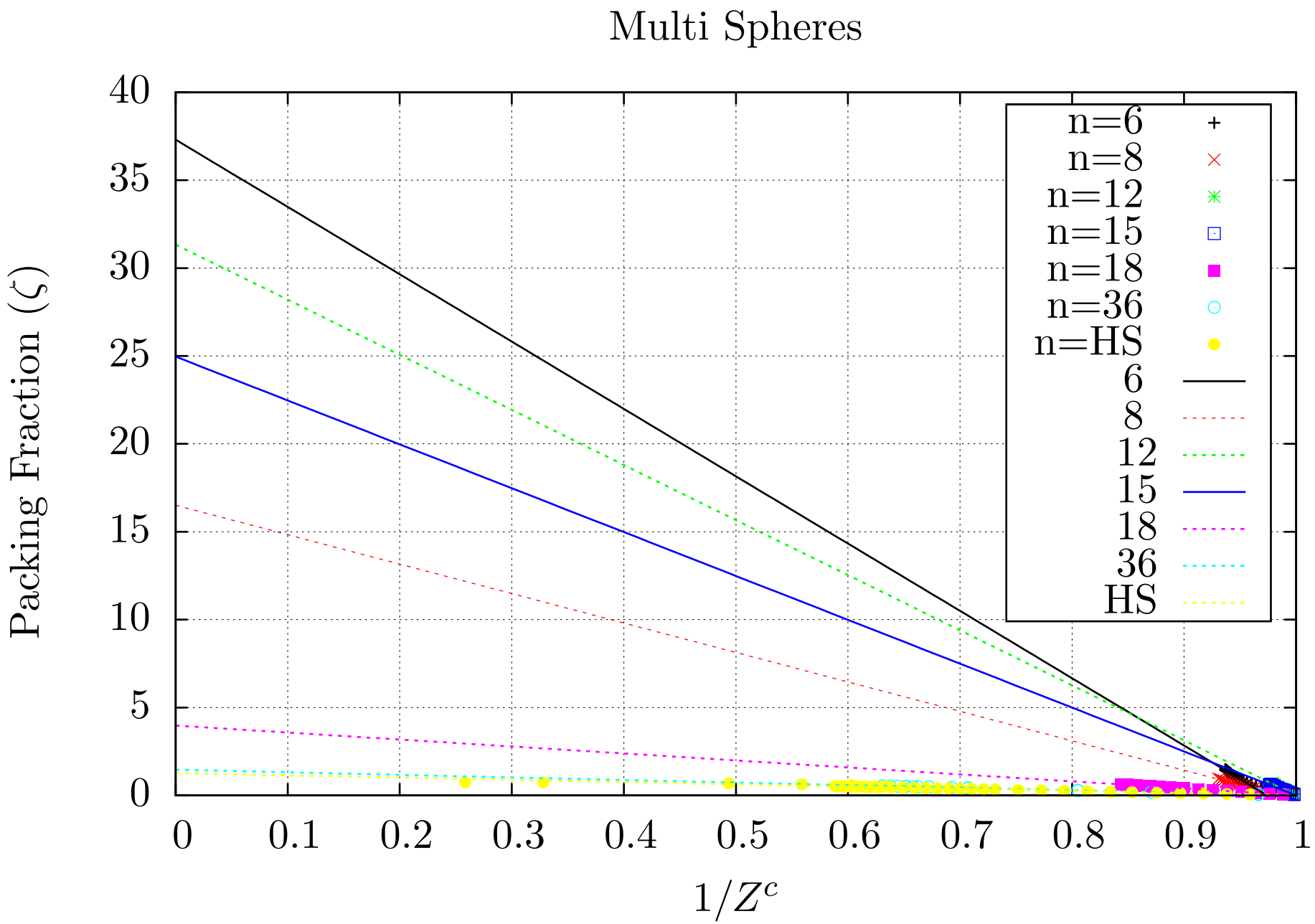

Figure 25: Superimposed graph of figs. 8 to 10, 14, 17, 20 and 23, taking into account the exclusions that were made to the data sets of $n = 6, 8, 12, 15$ and the hard sphere case ($n \to \infty$).

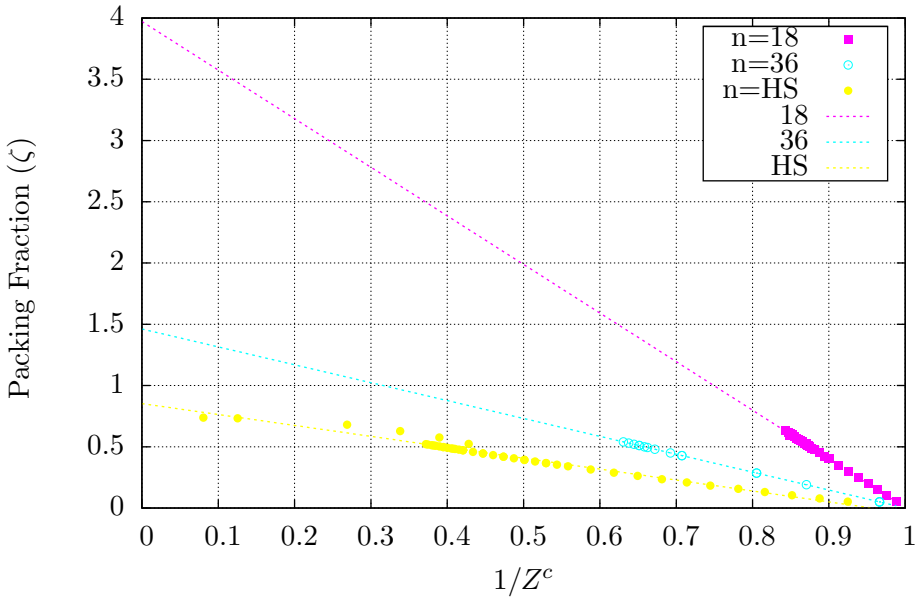

Figure 26: Grouped plot containing $n = 18, 36$ and the hard sphere case ($n \to \infty$).

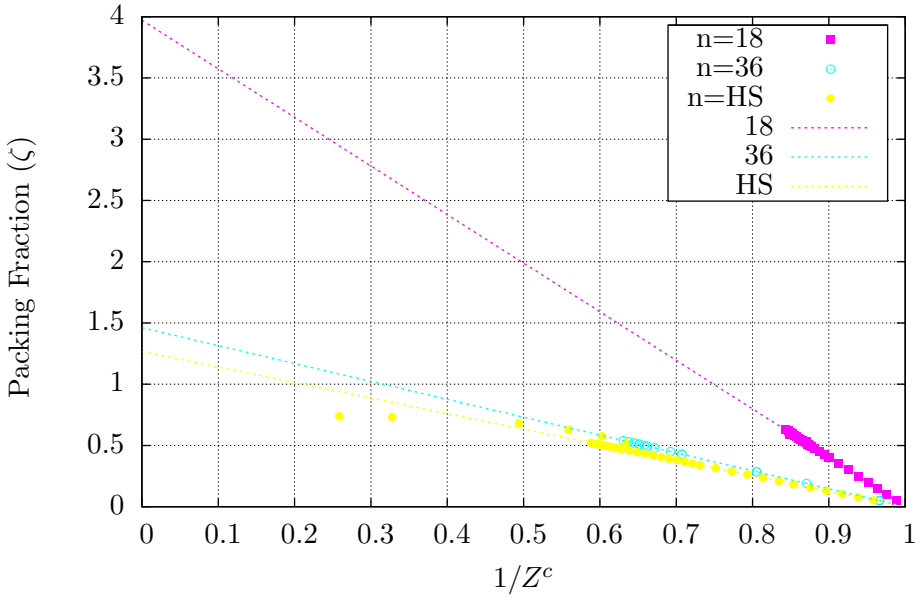

Figure 27: Same graph as fig. 26 with the points above $\zeta = 0.52$ excluded from the fitting range of the hard sphere data set.

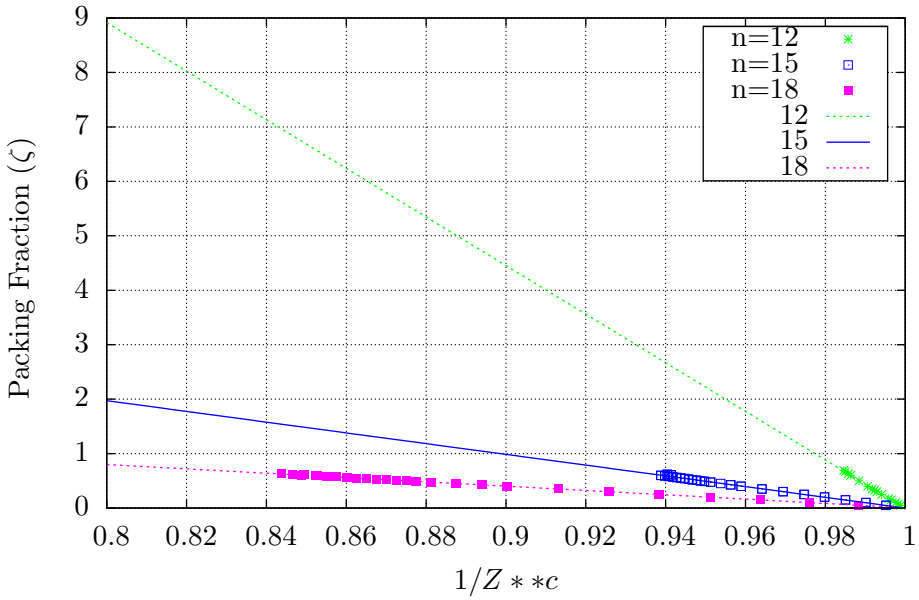

Figure 28: Grouped plot containing $n = 12, 15, 18$.

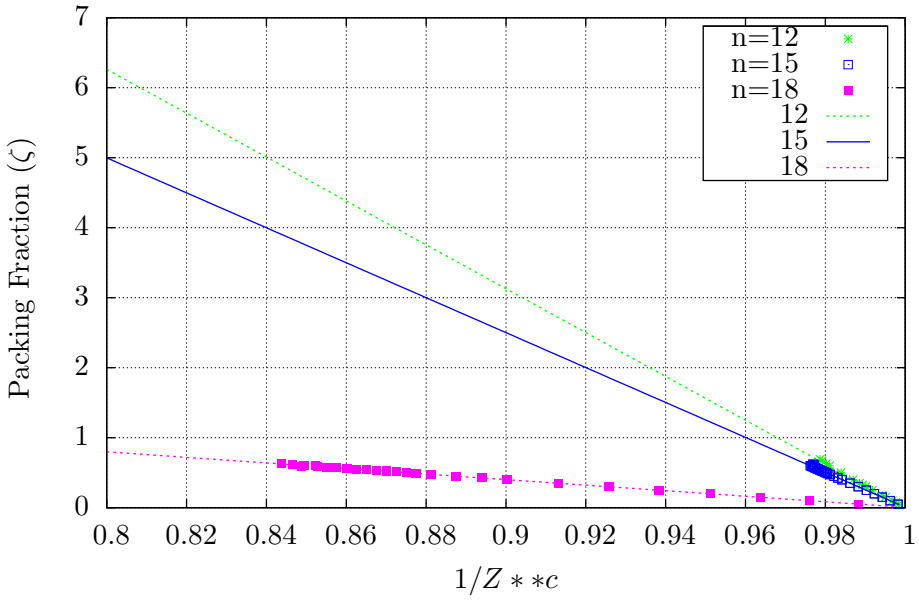

Figure 29: Same graph as fig. 28 with the points above $\zeta = 0.6$ excluded from the fitting ranges of the $n = 12, 15$ data sets.

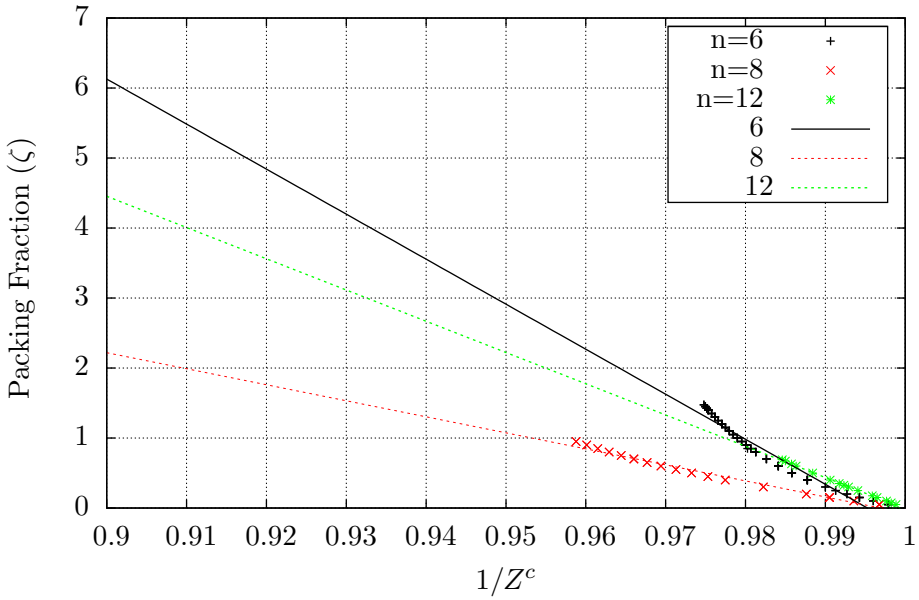

Figure 30: Grouped plot containing $n = 6, 8, 12$.

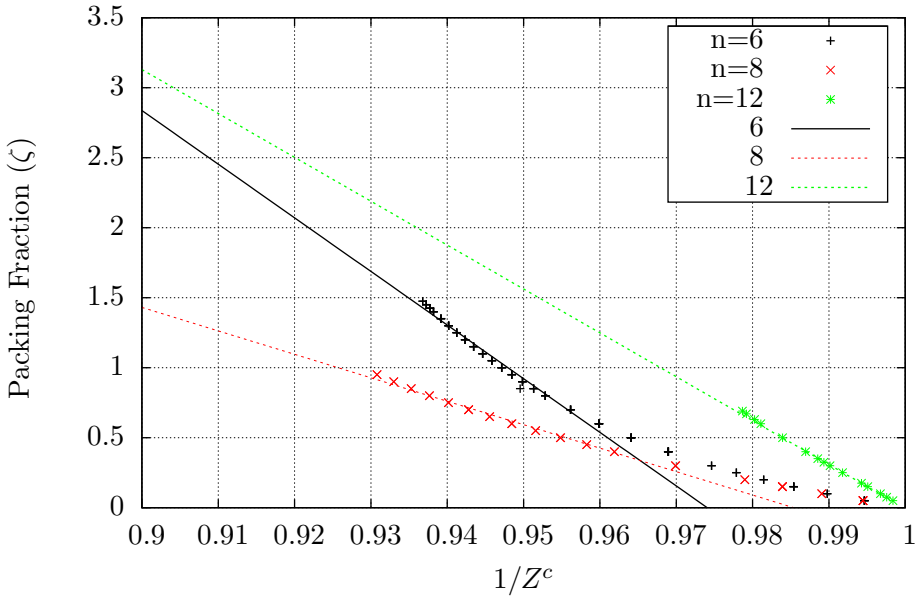

Figure 31: Same graph as fig. 30 with the points below $\zeta = 0.6, 0.3$ and above $\zeta = 0.6$ excluded from the fitting ranges of the $n = 6, 8$, and $n = 12$ data sets respectively.